Earth and Planetary Science Letters 560 (2021) 116806

Contents lists available at ScienceDirect

Earth and Planetary Science Letters

www.elsevier.com/locate/epsl

Experimental investigation of OH/H_2O in H^+-irradiated plagioclase: Implications for the thermal stability of water on the lunar surface

Xiandi Zeng [a,c], Hong Tang [a,b,d,*], XiongYao Li [a,b,d], Xiaojia Zeng [a], Wen Yu [a,b,d], Jianzhong Liu [a,b,d], Yongliao Zou [e]

[a] Center for Lunar and Planetary Sciences, Institute of Geochemistry, Chinese Academy of Sciences, Guiyang 550081, China
[b] CAS Center for Excellence in Comparative Planetology, Hefei, China
[c] University of Chinese Academy of Sciences, Beijing 100049, China
[d] Key Laboratory of Space Manufacturing Technology, Chinese Academy of Sciences, Beijing 100094, China
[e] National Space Science Center, Chinese Academy of Sciences, Beijing 100190, China

ARTICLE INFO

Article history:
Received 25 May 2020
Received in revised form 15 January 2021
Accepted 3 February 2021
Available online 12 February 2021
Editor: W.B. McKinnon

Keywords:
solar wind implantation
H^+ irradiation
thermal stability
lunar water

ABSTRACT

Determining the characteristics and thermal stability of solar wind-produced OH/H_2O is critical to understanding the formation and migration of water on the lunar surface. In this study, terrestrial plagioclase (An_{50-53}) was used as a lunar analogue and was irradiated with 5 keV H^+ at a fluence of $\sim 1\times10^{17}$ H^+/cm^2. The irradiated plagioclase was characterized via Fourier transform infrared spectroscopy, nanoscale secondary ion mass spectrometry, Raman spectroscopy, and transmission electron microscopy. The thermal stability of OH/H_2O in the irradiated plagioclase was investigated via heating experiments. Our results reveal (1) a ~100–200 ppm increase in the water content of the irradiated plagioclase; (2) structural hydrous species formation in the plagioclase through H^+ implantation, including Type I H_2O (~2.75 μm) and Type II H_2O (~2.90 μm); and (3) the escape of much of the OH/H_2O formed by H^+ implantation at a temperature equivalent to the highest temperature on the lunar surface. The results of this study can improve our understanding of OH/H_2O thermal stability on the lunar surface and provide a baseline for the interpretation of remote sensing observations.

1. Introduction

Solar wind-produced water was first proposed as one of the origins of lunar water by Zeller et al. (1966). Until recently, the Moon Mineralogy Mapper (M^3) on Chandrayaan-1, the Visual and Infrared Mapping Spectrometer (VIMS) on Cassini, and the High-Resolution Instrument infrared spectrometer on the Deep Impact satellites had all detected absorption near 2.8 to 3 μm, which indicates the presence of water (possibly related to hydroxyl and molecular water; Clark, 2009; Pieters et al., 2009; Sunshine et al., 2009). However, H_2O cannot be distinguished from OH in M^3 spectra with the longest wavelength of 2.976 μm (Li and Milliken, 2017). Data suggest that OH/H_2O on the Moon is present at concentrations of several thousand ppm (Clark, 2009; Pieters et al., 2009; Sunshine et al., 2009; Li and Milliken, 2017). The large variation in OH/H_2O content is most likely related to variations in latitude and temperature (Li and Milliken, 2017; Wöhler et al., 2017). In addition, secondary ion mass spectrometry (SIMS) measurements of lunar agglutinates reveal that solar wind can contribute up to 70–200 ppm of the hydroxyl groups on the Moon (Liu et al., 2012). Stephant and Robert (2014) also concluded that lunar hydroxyl groups mostly occur as a result of solar wind implantation, based on the deuterium/hydrogen (D/H) and $^7Li/^6Li$ ratios in the agglutinates, volcanic glasses, and plagioclase grains from Apollo samples.

Many laboratory experiments have been performed to examine the production of OH/H_2O through solar wind implantation on the lunar regolith (Zeller et al., 1966; Holmes et al., 1975; Cantando et al., 2008; Burke et al., 2011; Managadze et al., 2011; Ichimura et al., 2012; Schaible and Baragiola, 2015). Most of these experiments have included qualitative analyses of OH/H_2O formation (Managadze et al., 2011; Ichimura et al., 2012; Bradley et al., 2014), but the lack of quantitative analyses of the OH/H_2O produced by solar wind limits our knowledge of the mechanism of formation and contribution of solar wind-produced water on the Moon. Most experimental investigations have only identified the formation of hydroxyl groups during H^+ implantation (Yoshida et al., 2004; Schaible and Baragiola, 2015). However, Bradley et al. (2014) found

* Corresponding author at: Center for Lunar and Planetary Sciences, Institute of Geochemistry, Chinese Academy of Sciences, Guiyang 550081, China.
E-mail address: tanghong@vip.gyig.ac.cn (H. Tang).

https://doi.org/10.1016/j.epsl.2021.116806
0012-821X/

that H_2O forms in vesicles within the amorphous rims of plagioclase grains. The combination of protons from the solar wind and oxygen in the lunar silicates remains unknown, which limits further understanding of the formation and stability of solar wind-produced water.

The lunar surface temperature is believed to be a key factor affecting the retention, escape, and migration of solar wind-produced water, and yet experiments that investigate the effects of temperature on water stability are lacking (Poston et al., 2015; Wöhler et al., 2017; Hendrix et al., 2019). In this study, we investigated the thermal stability of solar wind-produced water on the lunar surface by using a terrestrial plagioclase analogue. In particular, we considered changes in the water content with temperature for H^+-irradiated plagioclase.

2. Methodology

2.1. Sample preparation

Plagioclase is one of the most common mineral phases on the lunar surface (Yan et al., 2010); in this study, we used terrestrial plagioclase, selected from the Damiao anorthosite (located in Hebei, China), as a lunar mineral analogue to conduct our experiments. Through electron microprobe (JEOL JXA-8230 electron microprobe EMP at the Guilin University of Technology) measurements, the studied plagioclase was identified as labradorite (An_{50-53}). To determine the water content using transmission infrared spectroscopy, double-sided polished sections of plagioclase with a size and thickness of ~1 × 1 cm and 200 ± 10 μm, respectively, were prepared. To eliminate any organic matter produced during the sample preparation, the polished samples were soaked in acetone for 24 h, cleaned with ethanol, and then washed with pure water. Finally, the samples were baked at ~110 °C for 24 h to remove any adsorbed water on the sample surfaces.

2.2. Ion irradiation

Experiments using H^+-irradiated samples were performed with an ion implanter at the Institute of Geochemistry, Chinese Academy of Sciences. This instrument consists of an ion source, a vacuum system, a magnetic analyzer, an accelerator, a sample chamber, and a control system. Ions (e.g., H^+) produced by the ionized H_2 gas are accelerated in an electric field. Then, the H^+ ions are passed through the magnetic deflection field and implanted onto the studied samples in an irradiation chamber. The irradiated area is ~1.5 cm^2. The energy of the implanted H^+ was 5 keV owing to the limits of the instrument's performance. This energy is slightly higher than the typical energy range of solar wind but is still suitable for simulating proton implantation (Schaible and Baragiola, 2015). The H^+ fluence was $1 \pm 0.03 \times 10^{17}$ H^+/cm^2, and the flux was $\sim 1.85 \pm 0.06 \times 10^{12}$ ions/cm^2·s, which is equivalent to 30 years of solar wind proton implantation on the Moon (Burke et al., 2011). The total irradiation time was ~10 h, and the irradiation temperature was 21 ± 1 °C (monitored by an infrared thermometer). During the irradiation processes, the pressure was controlled at $\sim 2 \times 10^{-7}$ Torr to simulate the high vacuum conditions of the lunar surface.

2.3. Fourier transform infrared spectroscopy

Transmission infrared spectra measurements of the samples were performed before and after irradiation using a Thermo IS50 Fourier transform infrared (FTIR) spectrometer coupled with a Continu μm IR microscope at the Institute of Geochemistry, Chinese Academy of Sciences. The transfer of the irradiated plagioclase samples between the irradiation chamber and the FTIR spectrometer occurred in the air, and the exposure time was less than 10 min, following which all samples were restored in the drying oven. Transmission spectra were obtained in the range of 4500–1000 cm^{-1} (i.e., 2.22–10 μm) with a spectral resolution of 4 cm^{-1}, averaged over 128 scans. For quantitative analyses of OH/H_2O, infrared absorption was measured in transmission before and after H^+ irradiation, at the same positions. Clean, crack-free, and alteration-free areas on each single crystal of plagioclase were chosen for FTIR measurements. Each measurement spot was ~50 × 50 μm in size.

Analyses of OH/H_2O characteristics were based on the FTIR data by comparing the spectra of samples before and after H^+ irradiation, especially the peak position and absorption area. Thus, we extracted FTIR spectra in the range of 4400–2400 cm^{-1}, including the vibration absorption wavelengths of OH and H_2O.

The content of OH/H_2O was quantitatively calculated in the range of 4400–2400 cm^{-1}. Baseline correction and multiple peak fitting were performed using the Origin 9.0 software. The Beer–Lambert rule, modified by Johnson and Rossman (2004), states that

$$\Delta = I \times c \times t \quad (1)$$

where Δ is the area integral of the OH/H_2O absorption peak, I is the molar absorption coefficient, t is the thickness (cm) of the sample, and c is the water content (ppm).

Here, the integral area ×3 was taken as Δ for unpolarized light measurement patterns (Kovács et al., 2008). The value of I is 107000 ± 5000 L·mol $(H_2O)^{-1}$·cm^{-2}, but in this study, the unit of I was replaced by ppm, and, therefore, its value was 15.3 ± 0.7 ppm·cm^{-2} (Johnson and Rossman, 2003).

Water content determination using the FTIR spectra can be affected by uncertainties in sample thickness (~5%), spectra baseline correction (~0.2%), unpolarized light measurements (~20%), and the absorption coefficient (~4.5%). Therefore, we estimated the uncertainty of the calculated water content to be ~30% (Kovács et al., 2008; Liu et al., 2012; Johnson and Rossman, 2003).

2.4. Nanometer-scale secondary ion mass spectrometry

The hydrogen isotopes and water content of the H^+ irradiated and the unirradiated plagioclase were measured *in situ* with a Cameca NanoSIMS 50L at the Institute of Geology and Geophysics, Chinese Academy of Sciences. The plagioclase grains were measured during the same session as an NWA 8657 standard (Hu et al., 2020a,b). The analytical conditions and data reduction are identical to those reported by Hu et al. (2020a, 2020b). The secondary ions of $^1H^-$, $^2D^-$, $^{12}C^-$, and $^{18}O^-$ were simultaneously counted using electron multipliers from the central areas (50% blanking). San Carlos olivine was used for H background corrections according to the following equations: $H/O_{bg} = (H_{counts} - H_{bg})/O_{counts}$), $D/H_{measured} = (1-f) \times D/H_{real} + f \times D/H_{bg}$, where f is the proportion of H from the instrument background (Tartèse et al., 2019; Hu et al., 2020a,b), $D/H_{bg} = (1.98 \pm 0.51) \times 10^{-4}$, and $H_{bg} = (1.60 \pm 0.31) \times 10^5$ (2SD, $N = 4$). The instrumental mass fractionation (IMF) and matrix effect on water content were established by measuring two apatite standards: Durango apatite (0.0478 wt% H_2O) (Greenwood et al., 2008, 2011) and Kovdor apatite (0.98 ± 0.07 wt% H_2O and $\delta D = -66 \pm 21‰$) (Nadeau et al., 1999), and one MORB glass reference material (SWIT MORB glass; 0.258 wt% H_2O and $\delta D = -73 \pm 2‰$). Hydrogen isotopic compositions are presented in delta notation, $\delta D = ((D/H)_{sample}/(D/H)_{SMOW}) - 1) \times 1000‰$, where SMOW is the standard mean ocean water with a D/H ratio of 1.5576×10^{-4}. Hu et al. (2014, 2015) outline additional technical details. All data are reported at 2σ uncertainties including the reproducibility of D/H measurements on reference materials, the uncertainty on H_2O background subtraction on San Carlos olivine and the internal precision of each analysis. Four spots were de-

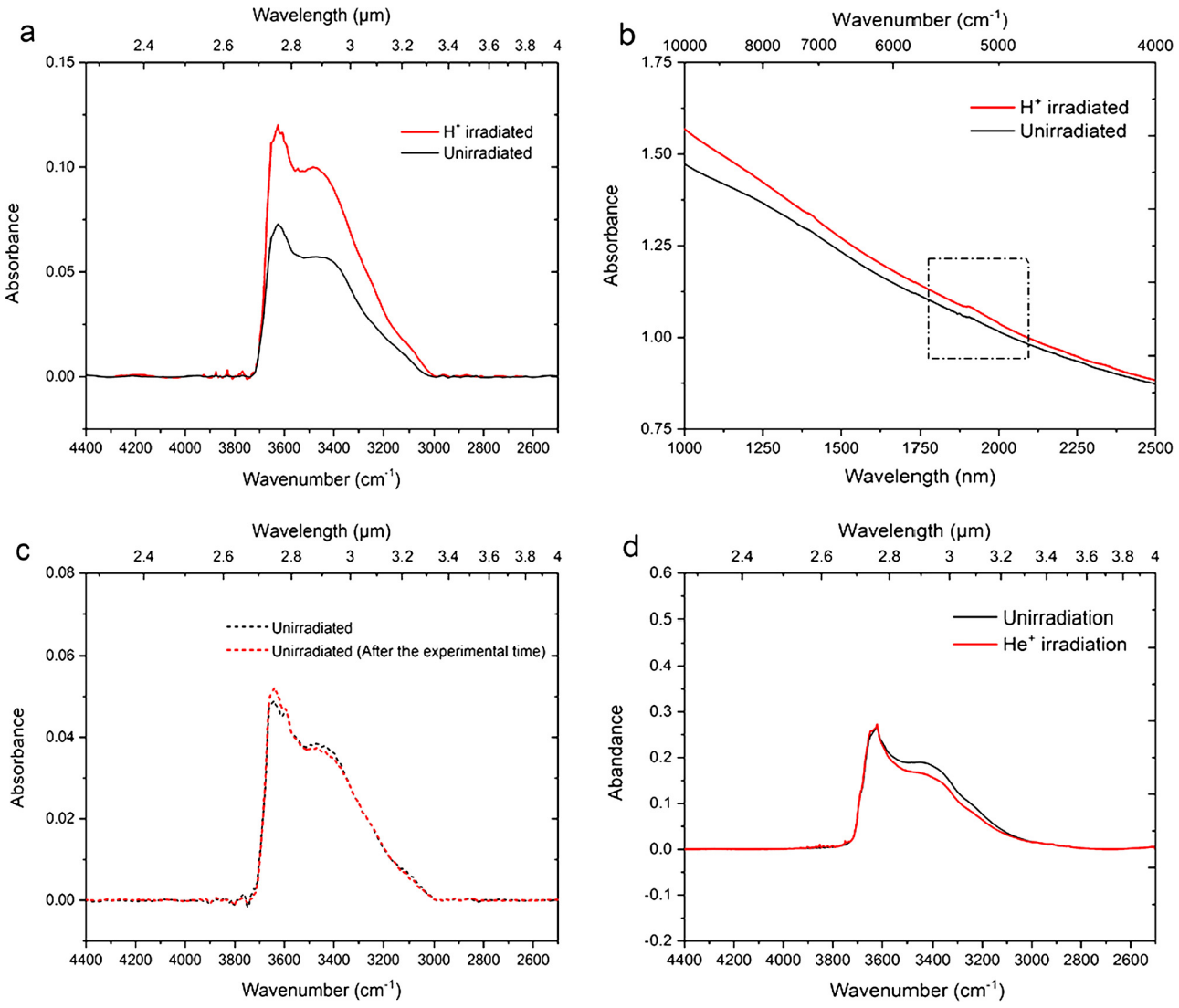

Fig. 1. Fourier transform infrared (FTIR) spectra. (a) Unirradiated and H^+-irradiated (5 keV) plagioclase; the absorption feature at 3000–3600 cm^{-1} in the unirradiated sample represents the initial water in the plagioclase. (b) The absorption at ~5200 cm^{-1} represents the combination band of H_2O in the Unirradiated and H^+-irradiated (5 keV) plagioclase. (c) FTIR spectra of the unirradiated reference sample. (d) The change of absorption spectra before and after He^+ irradiation (5 keV). (For interpretation of the colors in the figure(s), the reader is referred to the web version of this article.)

termined for H^+ irradiated and unirradiated plagioclase and the analytical depth was approximately 1.3 μm.

2.5. Raman spectroscopy

To reveal the difference between the molecular bonding before and after H^+ irradiation in the plagioclase, Raman spectra were collected from the same positions in the sample using a Renishaw InVia Laser Raman Spectrometer at the Institute of Geochemistry, Chinese Academy of Sciences. The spectral detection parameters were as follows: laser wavelength of 532 nm, spot size of <1 μm, and exposure time of 20 s; the spectra were accumulated twice. After data collection, Origin 9.0 software was used for spectral processing.

2.6. Transmission electron microscopy

To observe the structural damages in the H^+-irritated plagioclase, transmission electron microscopy (TEM) was used to analyze the microstructure of the uppermost layer. A thin (~70 nm) slice of irradiated plagioclase was prepared using a FEI Scios dual-beam focused ion beam/scanning electron microscope at the Institute of Geochemistry, Chinese Academy of Sciences. Analyses were performed using a Talos F200S TEM at the Guangdong University of Technology. The instrument was operated at an accelerating voltage of 200 kV and a beam current of 1 nA.

2.7. Heating experiments

To investigate the thermal stability of OH/H_2O in irradiated plagioclase, a heating experiment was performed using *in situ* hot-stage FTIR microspectroscopy. We performed a heating experiment from 20 °C to 1000 °C under nitrogen purge. For the lower temperature range (i.e., 20 °C to 300 °C), irradiated plagioclase was heated and measured through FTIR microspectroscopy with an interval of 40 °C. Then, the sample was heated and measured using FTIR microspectroscopy from 300 °C to 1000 °C at 100 °C intervals. Finally, FTIR spectra were collected after the sample was cooled to 20 °C.

3. Results and discussion

3.1. Water content variation after H^+ irradiation

Fig. 1a shows the baseline-corrected FTIR absorbance spectra for plagioclase before and after H^+ (5 keV) irradiation. Plagioclase

Table 1
Absorption and water contents of unirradiated and H^+-irradiated (5 keV) plagioclase.

Analyzed positions	Unirradiated plagioclase					H^+ irradiated (5 keV) plagioclase					Δ[b] (ppm)		
	Peak-1 (cm^{-1})	Peak-2 (cm^{-1})	Peak area-1 (cm^{-1})	Peak area-2 (cm^{-1})	Water content[a] (ppm)	Peak-1 (cm^{-1})	Peak-2 (cm^{-1})	Peak area-1 (cm^{-1})	Peak area-2 (cm^{-1})	Water content[a] (ppm)	Peak-1	Peak-2	Total
1	3625	3457	5.13	21.33	259 ± 17	3625	3455	7.88	36.12	431 ± 29	27	145	172 ± 34
2	3620	3450	6.61	16.34	225 ± 15	3625	3447	8.82	24.55	327 ± 22	22	80	102 ± 26
3	3637	3470	17.62	49.00	653 ± 44	3633	3459	21.28	66.13	857 ± 58	36	168	204 ± 73
4	3629	3449	3.15	7.94	109 ± 7	3639	3463	8.93	21.47	298 ± 20	56	133	189 ± 21
5	3629	3459	6.41	24.13	299 ± 20	3629	3465	11.02	38.19	482 ± 32	45	138	183 ± 38
6	3644	3459	5.99	21.39	268 ±18	3629	3459	10.76	31.31	412 ± 27	47	97	144 ± 33

[a] Water content includes water abundance in peak-1 and peak-2, which are calculated using formula (1) shown in section 2.3. The error is from thickness, baseline correction, and absorption coefficient in formula (1), and has been calculated using uncertainty propagation.
[b] Δ represents the changes in water content after H^+ implantation in plagioclase compared with the water content in unirradiated plagioclase.

before H^+ irradiation showed initial water absorption at ~3600 cm^{-1} and 3400 cm^{-1}, whereas H^+-irradiated plagioclase exhibited an obviously increased absorption. To determine the influence of environmental water on the implanted samples, two different background samples were prepared. The first background sample was an unirradiated plagioclase that was exposed to air for the same time period as the irradiated sample. A plagioclase slice was irradiated by 5 keV He^+ with 1 ± 0.3 × 10^{17} ions/cm^2 as the other background sample. There was little change (<1 ppm water variation) in the unirradiated plagioclase after the same experimental exposure time as the irradiated plagioclase (Fig. 1c). Fig. 1d shows that the absorption at 3449 cm^{-1} decreased, whereas the peak of 3624 cm^{-1} was unchanged in the plagioclase sample after the He^+ irradiation. The total reduced water content was 53 ± 16 ppm, which was caused by the sputtering of H and O atoms in the outermost layer of the plagioclase during the He^+ irradiation. Therefore, the enhancement at the 3000–3700 cm^{-1} absorption range in the plagioclase sample after H^+ irradiation can be attributed entirely to OH/H_2O formation by the implanted H^+.

The water content variation after H^+ irradiation was then calculated according to formula (1). Table 1 summarizes the absorption features and content of water in unirradiated and H^+-irradiated (5 keV) plagioclase samples at six different analysis positions. The increased water content in the plagioclase after H^+ irradiation ranged from 102 ± 26 to 204 ± 73 ppm. The differences in water content in different positions are likely related to crystal orientations. According to Li et al. (2013), implanted He^+ in different crystal planes of olivine caused different degrees of crystal structural damage. As such, H^+ implanted into different crystal planes of plagioclase could also affect the retention of H ions and water formation, resulting in the observed differences in the increases in water content for different positions of the plagioclase.

Fig. 2 shows the water content calculated by $^1H/^{18}O$ ratios at four spots for unirradiated and H^+-irradiated (5 keV) plagioclase. The values of water content in the unirradiated sample were 28 ± 2–62 ± 5 ppm, while those in the H^+ irradiated sample were 124 ± 10–192 ± 13 ppm. The increased water content at four analyzed positions exhibited ~115 ppm after H^+ irradiation, consistent with the FTIR data. The D/H ratios from 300 counts in each measured point were measured successively in the 1.3 μm depth range (Fig. 3). Except for data with a value of zero, the D/H ratios of H^+-irradiated plagioclase were mainly distributed in the range of 3–3.5 × 10^{-4}, which was relatively lower than that of the unirradiated samples (D/H ratios mainly in the range of 8.3–12.3 × 10^{-4}). This indicates that implanted H^+ was effectively retained in the plagioclase, thereby reducing the D/H ratio in the sample. In addition, a slight increase of the D/H ratio from the rim to the interior indicates a strong diffusion capability of H during the irradiation process.

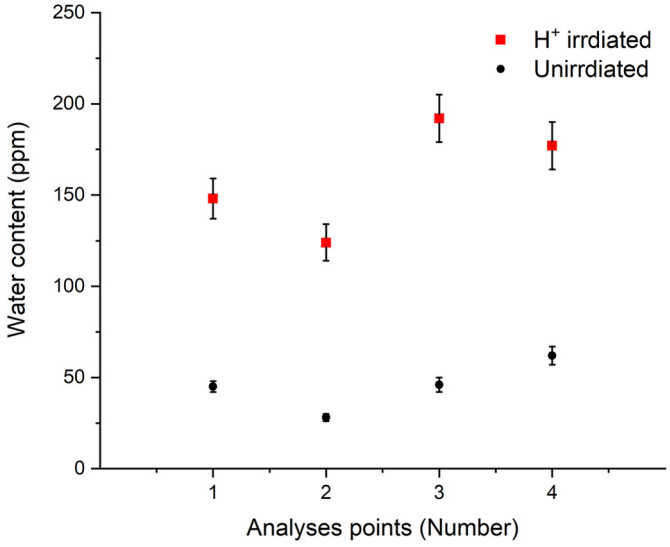

Fig. 2. The water content calculated by $^1H/^{18}O$ at four analyzed spots for unirradiated and H^+-irradiated (5 keV) plagioclase. Error bars represent 2σ standard deviations and uncertainties.

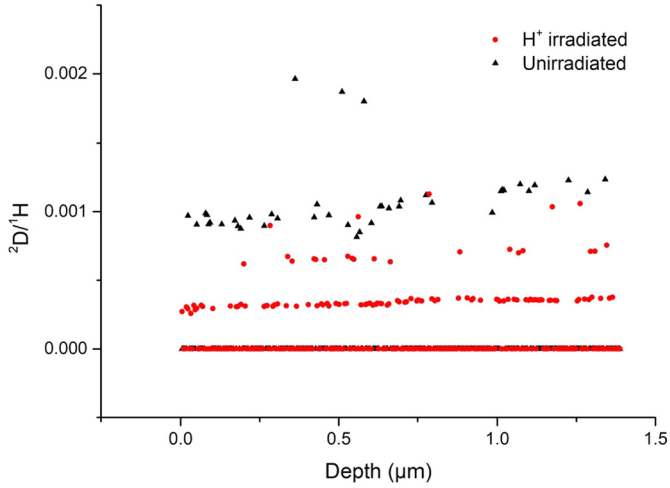

Fig. 3. The deuterium/hydrogen (D/H) ratios as a function of depth for unirradiated and H^+-irradiated (5 keV) plagioclase.

FTIR spectra and NanoSIMS data for unirradiated and H^+-irradiated (5 keV) plagioclase exhibit a ~100–200 ppm increase in the water content after H^+ implantation. Our results are not only consistent with the water content evaluated by the orbital IR spectra data (VIMS, 10–1000 ppm; M^3, ~500–750 ppm; DI, <5000 ppm; Clark, 2009; Li and Milliken, 2017; Sunshine et al., 2009),

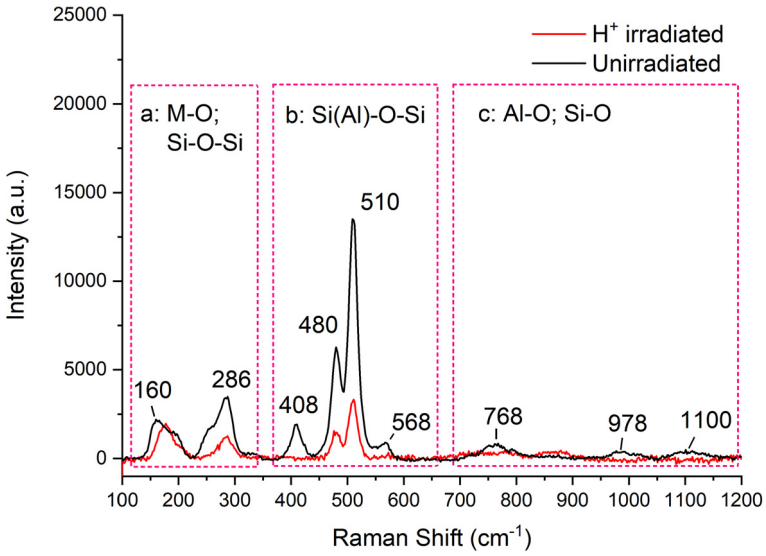

Fig. 4. Representative Raman spectra of unirradiated and H^+-irradiated (5 keV) plagioclase. Marked on the skeleton range are (a) the metal-oxygen bond vibrations (160 cm^{-1}) and bending vibration of Si-O-Si (286 cm^{-1}), (b) Si(Al)–O–Si bridging oxygen bending vibration range, and (c) Si(Al)–O non-bridging oxygen stretching vibration range (Frogner et al., 1998).

but also with those of Apollo samples analyses (Liu et al., 2012; Stephant and Robert, 2014). The average increased band depth in transmittance was 6.22% for the plagioclase after H^+ irradiation (5 keV). The growth of OH/H_2O absorption depth in this study is similar to that in an implantation experiment conducted on Apollo 16 soil (40% plagioclase) with 1.1 keV and $\sim 10^{21}$ ions/m^2 fluence (close to $1 \pm 0.03 \times 10^{17}$ H^+/cm^2 in this study) H^+ (Ichimura et al., 2012). This suggests that solar wind-produced water is an important contributor to lunar surface water, and that plagioclase is a critical mineral for the formation of water through solar wind implantation.

3.2. Water occurrence after H^+ irradiation

The FTIR spectra of both unirradiated and H^+-irradiated (5 keV) plagioclase show two peaks related to water, one at 3620 cm^{-1} and the other at 3450 cm^{-1} (Table 1). These two intense bands, with H–O–H fundamental frequency vibrations in the range of 3400–3700 cm^{-1} and the combination band of H–O–H around 5200 cm^{-1} (Fig. 1a, b), represent the structural hydrous species: Type I H_2O ($\sim$3639 cm^{-1}; i.e., 2.75 μm) and Type II H_2O ($\sim$3445 cm^{-1}; i.e., 2.90 μm) (Aines and Rossman, 1985; Johnson and Rossman, 2004). It is important to note that Type I H_2O and Type II H_2O are not the free molecular water mentioned in Clark (2009). Type I H_2O and Type II H_2O are both structural bound H_2O in plagioclase (Kronenberg et al., 1996). The mechanism for H incorporation for both Type I H_2O and Type II H_2O is bonding to the O atoms adjacent to M-site vacancies (e.g., Ca, Na) (Johnson and Rossman, 2004). Another possibility is that these two structural H_2O types are accommodated within the crankshaft-like chains that run parallel to the a-axis (Johnson and Rossman, 2004). However, Type I H_2O at $\sim$3600 cm^{-1} might also be related to tetrahedral vacancies (i.e., Si and Al defects) (Mosenfelder et al., 2020). The increase in the content of Type II H_2O is significantly higher than that of Type I H_2O (see Table 1), which means that Type II H_2O was likely formed more easily. Furthermore, although the water absorbance of H^+-irradiated plagioclase was higher than that of unirradiated plagioclase, the peak positions were almost the same. This indicates that implanted H^+ that combined with oxygen in the plagioclase to form water was preferentially retained in the original structural locations. As Johnson and Rossman (2004) discussion, there are three types (I, IIa and IIb) structural OH and two types (I and II) structural H_2O in plagioclase. If the chosen plagioclase samples contained other types of OH/H_2O or no OH/H_2O, then the types of OH/H_2O formed after H^+ implantation would be different. However, the absorption range (3200–3800 cm^{-1}) of the OH/H_2O, which represents the fundamental frequency vibrations of O–H and H–O–H, was basically the same.

Fig. 4 shows the baseline-corrected Raman spectra for unirradiated and H^+-irradiated (5 keV) plagioclase. The Raman spectra of plagioclase in the range of 100–1200 cm^{-1} can be divided into three regions, representing the vibrations of M–O and bending vibrations of Si-O-Si (100–300 cm^{-1}), Si(Al)–O–Si(Al) (400–700 cm^{-1}), and Si(Al)–O (750–1200 cm^{-1}) (Frogner et al., 1998). Compared with the spectra of unirradiated plagioclase, most of the peaks in the H^+-irradiated plagioclase decreased, and some even disappeared. The peaks at 480 cm^{-1} and 510 cm^{-1} represent the four-membered ring of a tetrahedral structure (Freeman et al., 2008); they clearly decreased, and some peaks related to silica-oxygen bonds (e.g., 768 cm^{-1}, 568 cm^{-1}, and 408 cm^{-1}) even disappeared from the spectra. This indicates that the tetrahedral skeleton suffered serious deformation and amorphization (Brunetto and Strazzulla, 2005; Li et al., 2013).

TEM and high-resolution TEM images of the surface H^+-irradiated (5 keV) plagioclase are presented in Fig. 5. There was an irregular 20–150 nm thick amorphous rim on the uppermost surface, which was slightly deeper than that observed on lunar soil grains (Keller and McKay, 1997). This large maximum depth may, in part, be due to the high energy (5 keV) used in the experiment (not 1 keV, as observed in solar wind energy). This irregular rim may have been caused by the inhomogeneity of the microstructure and element content in plagioclase. The irradiated damage region was typically completely amorphous; however, partial amorphization occurred near the boundary region. The amorphization on the surface of H^+-irradiated plagioclase indicated that the structure had been destroyed, and that a large number of defects and vacancies had been produced, making it easy to retain the implanted H^+ (Farrell et al., 2015). The sample was completely crystalline below the boundary and was not affected by H^+ implantation.

From the Raman spectra and TEM images, we conclude that the surface of H^+-irradiated (5 keV) plagioclase suffered serious structural damage, to a maximum depth of 150 nm, after H^+ im-

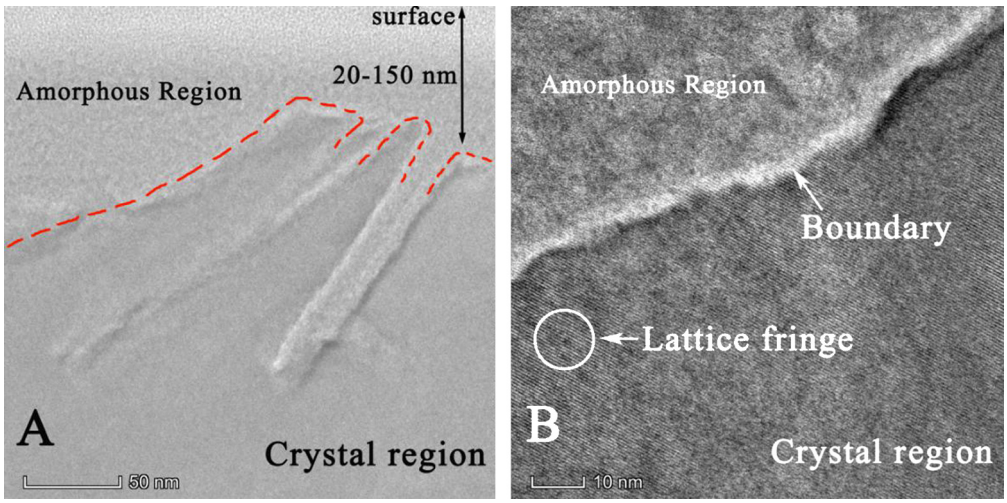

Fig. 5. TEM images of H^+-irradiated (5 keV) plagioclase include amorphous region (rim) and crystal region. (a) Transmission electron microscope (TEM) and (b) high resolution TEM images.

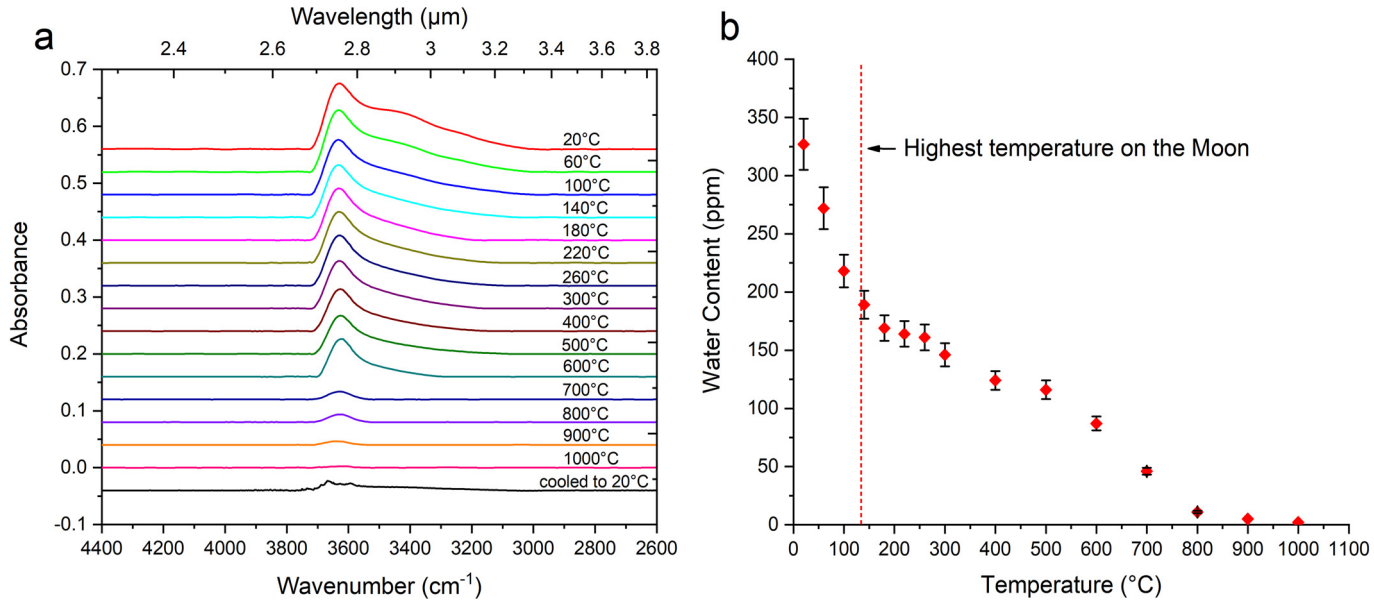

Fig. 6. FTIR spectra and variations in water content of H^+-irradiated (5 keV) plagioclase. (a) FTIR spectra of H^+-irradiated (5 keV) plagioclase under different heating temperatures (20–1000 °C and cooled to 20 °C), (b) Total water content variation with increasing temperature for H^+-irradiated (5 keV) plagioclase. The error bars are calculated by uncertainty propagation.

plantation. Damage at this depth would create many defects and vacancies and would result in abundant dangling oxygen bonds, which could then trap the implanted H^+ and combine to form OH/H_2O (McCord et al., 2011). In addition, the rapid mobility of H^+ could have allowed it to enter the deeper mineral structure and become trapped in pre-existing defects and dislocations. This is consistent with the occurrence of both Type I H_2O and Type II H_2O in the FTIR spectra. However, the specific combination site of implanted H with oxygen in the plagioclase structure and its relationship with structural damage needs to be studied further.

3.3. Water content as a function of temperature

The heating experiment for H^+-irradiated (5 keV) plagioclase demonstrated that both water peaks decreased with increasing temperature (Fig. 6a). The change in total water content with temperature (Fig. 6b and Table 2) demonstrated three stages of structural H_2O loss: a significant decrease between 20 °C and 180 °C, a gradual decrease between 180 °C and 500 °C, and a clear decrease between 500 °C and 1000 °C. This suggests that the loss of water content with temperature depends on water occurrence.

Fig. 7 and Table 2 show the content variations of Type I H_2O and Type II H_2O with increasing temperature for H^+-irradiated (5 keV) plagioclase; these content variations differed, especially in the range of 20 °C to 180 °C. As the temperature increased, the content of Type II H_2O (at ~3450 cm^{-1}) decreased sharply between 20 °C and 140 °C and eventually disappeared at 800 °C, whereas the content of Type I H_2O (at ~3630 cm^{-1}) decreased relatively slowly and did not disappear until 1000 °C. When the temperature increased to 140 °C, Type I H_2O was reduced by only 16 wt%, whereas the content of Type II H_2O was reduced by 51 wt%. The thermal stability of Type I H_2O and Type II H_2O differed; the former was more stable, similar to the findings of Aines and Rossman (1985).

The differences in temperature dependence of OH/H_2O in minerals are related to many conditions (e.g., chemical compositions,

Table 2
Water content variation as a function of increasing temperature for H^+-irradiated (5 keV) plagioclase.

Temperature (°C)	Type I H_2O			Type II H_2O			Total water content (ppm)
	Peak-1 (cm^{-1})	Peak area-1 (cm^{-1})	Water content (ppm)	Peak-2 (cm^{-1})	Peak area-2 (cm^{-1})	Water content (ppm)	
20	3625	8.82	86 ± 5	3447	24.55	241 ± 16	327 ± 22
60	3626	8.54	83 ± 5	3459	19.23	189 ± 12	272 ± 18
100	3633	7.42	72 ± 4	3480	14.91	146 ± 10	218 ± 14
140	3628	7.41	72 ± 4	3487	11.91	117 ± 8	189 ± 12
180	3629	7.13	70 ± 4	3494	10.19	99 ± 7	169 ± 11
220	3627	7.11	70 ± 4	3496	9.70	94 ± 6	164 ± 11
260	3626	7.03	69 ± 4	3498	9.42	92 ± 6	161 ± 11
300	3627	6.50	63 ± 4	3504	8.45	83 ± 5	146 ± 10
400	3625	5.70	56 ± 3	3505	6.96	68 ± 4	124 ± 8
500	3623	5.22	51 ± 3	3505	6.63	65 ± 4	116 ± 8
600	3624	4.74	46 ± 3	3530	4.21	41 ± 3	87 ± 6
700	3625	2.95	28 ± 2	3545	1.83	18 ± 1	46 ± 3
800	3627	1.22	11 ± 1	–	–	–	11 ± 1
900	3636	0.58	5 ± 0	–	–	–	5 ± 0
1000	3628	0.22	2 ± 0	–	–	–	2 ± 0

'–': No data.

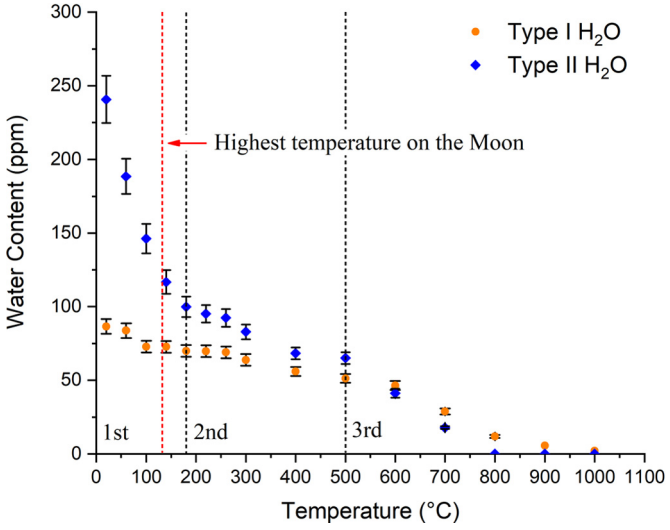

Fig. 7. Variations in Type I H_2O and Type II H_2O content with increasing temperature for H^+-irradiated (5 keV) plagioclase. The red dashed line represents the highest temperature on the Moon. The black dashed lines represent the three stages of water loss with temperature.

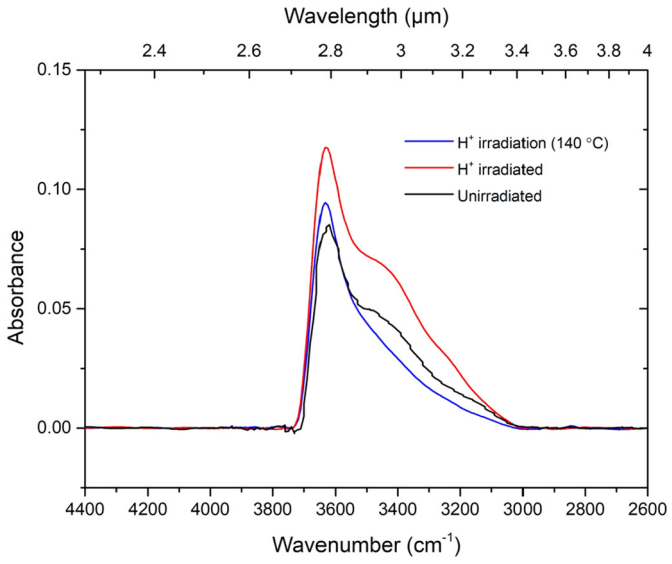

Fig. 8. FTIR spectra of unirradiated plagioclase (black line), H^+-irradiated (5 keV) plagioclase (red line), and H^+-irradiated (5 keV) plagioclase heated to 140 °C (blue line).

hydrogen storage sites) (Yang et al., 2019). Aines and Rossman (1985) simply analyzed that Type II H_2O occupying the open sites or defects was easily exchanged, while Type I H_2O occupied the more "structural" and well defined sites. Jones et al. (2018) had discussed the activation energies for the thermal dermal desorption of water and suggested that recombinative desorption (RD) was the primary loss of surface water. This process froms gas-phase water while "healing" the defect with a bridged oxygen bond in mineral: M-OH + M-OH → M-O-M + H_2O (g) (M is metal cation). The temperature required for a significant loss of -OH via second-order RD from metal oxides is different, for example, the peak RD temperature of SiO_2 (327 °C) is much higher than that of other metal oxides (e.g. Al_2O_3: ~ 77 °C). The loss of Type I and II H_2O may be explained by the RD theory. The different binding positions of Type I H_2O and Type II H_2O would determine the peak RD temperatures, resulting in their desorption temperature.

As discussed above, the H incorporation of Type I H_2O and Type II H_2O occurred via its bonding to O atoms adjacent to the M-sites (e.g., Ca and Na), whereas the Type I H_2O may also be related to the T-sites (e.g., Si and Al). According to Raman data, the four-membered tetrahedral rings suffered severe deformation, which would have changed the bond energy and the thermal stability of structural H_2O in H^+-irradiated plagioclase. Type I H_2O is relatively stable compared to Type II H_2O under a gradually rising temperature, which might be due to the H_2O being incorporated into different active sites or defects (Aines and Rossman, 1985; Jones et al., 2018). Thus, the binding position of structural H_2O, which influences the RD process, is very important for the thermal stability of water. Meanwhile, the effects of H^+ implantation on the plagioclase structure, which change the binding energy, should also be considered; this requires further study.

The FTIR spectra of unirradiated plagioclase, H^+-irradiated (5 keV) plagioclase, and H^+-irradiated (5 keV) plagioclase heated to 140 °C (Fig. 8) exhibited different structural H_2O absorptions. The unirradiated plagioclase showed characteristic structural H_2O absorption, whereas the absorption of H^+-irradiated plagioclase increased significantly at the original absorption position; however, the structural H_2O absorption of H^+-irradiated plagioclase heated to 140 °C decreased significantly. Compared with the unirradiated plagioclase, Type I H_2O absorption was higher for the H^+-irradiated plagioclase heated to 140 °C, whereas Type II H_2O absorption generally disappeared. This indicates that Type II H_2O

formed by H^+ implantation had completely disappeared, whereas residual Type I H_2O formed by H^+ implantation remained after being heated to 140 °C.

3.4. Implications for OH/H_2O thermal stability on the Moon

Our experiment results reveal that the water content of plagioclase formed by H^+ implantation was ~ 100–200 ppm in about 30 years, which indicated that solar wind proton implantation can produce hundreds of ppm or even more of water on the lunar surface, which is consistent with previous analysis of lunar infrared spectra and lunar samples (e.g., Liu et al., 2012; Li and Milliken, 2017). Moreover, the OH/H_2O absorption is closely related to latitude and temporal variation from the lunar infrared spectra analyses. That is, the OH/H_2O absorption gradually increases from the equator to the poles, and the OH/H_2O absorption reaches maximum value in the morning/evening and minimum value at the noon (Sunshine et al., 2009; McCord et al., 2011; Li and Milliken, 2017). Hurley et al. (2015) and Williams et al. (2016) calculated the correlation between temperature and latitude of lunar surface. On the lunar surface, the maximum temperature at the lunar equator is ~130 °C, whereas the highest temperatures for the mid-latitude regions are 60–90 °C. This indicates that temperature primarily controls the variation of OH/H_2O content on the lunar surface.

The structural H_2O formed by H^+ implantation in plagioclase decreased with increasing temperature, and the changes observed in Type I H_2O and Type II H_2O were different. Between 20 °C and 140 °C, the content of Type II H_2O decreased significantly, whereas the content of Type I H_2O decreased only slightly. According to the calculated water contents in the experiments at different temperatures, we assume that the escape rate between the original water and the water formed by H^+ implantation in plagioclase was the same as in the heating process. Combined with the maximum temperatures at different latitudes of the lunar surface, the maximum losses of OH/H_2O formed by solar wind proton implantation in low and middle latitudes would be ~42% and 17%–33%, respectively. For Type I H_2O at ~2.75 μm absorption formed by solar wind proton implantation, the maximum losses in low and middle latitudes would be ~16% and 3%–16%, respectively, whereas for the losses of the Type II H_2O at ~2.90 μm absorption, these would be ~51% and 22%–39%, respectively. Considering that lunar minerals basically contain little or no intrinsic water, if OH/H_2O formed after H^+ implantation were to escape preferentially during heating, then solar wind-produced water could be preserved at <10% in the equatorial region. The Type II H_2O at ~2.90 μm absorption would completely escape from the plagioclase, and ~36% of the Type I H_2O at ~2.75 μm absorption would remain. This result is consistent with the ~2.8 μm absorption that has been identified on the whole lunar surface; however, near 3 μm absorption is absent from the lunar equator (Clark, 2009; Sunshine et al., 2009). In our experiments, intrinsic structural H_2O in the plagioclase samples had a certain influence on the estimated extent of water escape after H^+ implantation. It is necessary to select samples with little or no water for performing experiments in future studies.

Furthermore, the formation and loss of OH/H_2O on the lunar surface reveals a dynamic hydration process. The experimental simulation of 30 years of H^+ implantation and heating in this study did not entirely represent the daily hydration and dehydration process. However, our results provide an important indication of the observed temperature dependence of lunar OH/H_2O. The continuous formation of water to supplement the water loss with temperature needs to be considered, particularly when studying the migration of water on the lunar surface.

In summary, Type I H_2O is more stable than Type II H_2O and could easily be retained on the lunar surface, which is consistent with the remote sensing observation data (Wöhler et al., 2017). The results of this study provide a useful baseline for analyzing the spatial and temporal variations in infrared spectra of OH/H_2O absorption observed by the Cassini, Deep Impact, and Chandrayaan-1 satellites.

4. Conclusions

In this study, terrestrial plagioclase (An_{50-53}) was irradiated with 5 keV H^+ to simulate the formation of OH/H_2O through solar wind implantation on the Moon. The content variation and occurrence of OH/H_2O in the irradiated plagioclase was characterized using FTIR spectrometry, Raman spectroscopy, NanoSIMS, and TEM. The heating experiment was conducted to investigate thermal stability of OH/H_2O.

Our results reveal that the increased water content in irradiated plagioclase was ~100–200 ppm. The structural H_2O formed by H^+ irradiation included both Type I H_2O (at ~3620 cm^{-1} in the FTIR spectra) and Type II H_2O (at ~3450 cm^{-1} in the FTIR spectra), which were accommodated through coupled substitutions at the M sites. Type I H_2O may also be related to the presence of Si and Al defects. Heating experiments suggested that much of the structural H_2O formed by H^+ implantation would be lost at 140 °C (similar to the highest temperature on the Moon). Type I H_2O was more stable than Type II H_2O and could be preserved on the Moon. The binding position of H_2O and the effect of H^+ implantation on the mineral structure were both found to be very important factors regarding the thermal stability of water. These data indicate that temperature variation is a critical influence that affects the retention of solar wind-produced OH/H_2O on the Moon.

This work provides an experimental reference for revealing the thermal stability of OH/H_2O on the lunar surface; the results also provide a baseline from which the remote sensing observations (e.g., M^3 spectra) can be interpreted. However, significant ambiguity remains as to the formation mechanism, retention, and migration of OH/H_2O formed by solar wind (e.g., the effects of irradiation flux on water formation in different lunar mineral species). Further lunar sample analyses and laboratory experiments with different mineral samples are needed to address these questions.

CRediT authorship contribution statement

Xiandi Zeng: Data curation, Investigation, Methodology, Software, Writing – original draft. **Hong Tang:** Conceptualization, Funding acquisition, Project administration, Resources. **XiongYao Li:** Funding acquisition, Supervision, Writing – review & editing. **Xiaojia Zeng:** Software, Writing – review & editing. **Wen Yu:** Funding acquisition, Investigation, Validation. **Jianzhong Liu:** Funding acquisition. **Yongliao Zou:** Funding acquisition.

Declaration of competing interest

The authors declare that they have no known competing financial interests or personal relationships that could have appeared to influence the work reported in this paper.

Acknowledgements

This work was supported by the Strategic Priority Research Program of Chinese Academy of Sciences [grant number XDB 41000000], National Natural Science Foundation of China [grant

numbers 41773066, 41931077], Youth Innovation Promotion Association CAS awards to Hong Tang [grant number 2018435], Xiongyao Li [grant number 2014359], Technical Advanced Research Project of Civil Space [grant number D020201], Key Research Program of Frontier Sciences [grant number QYZDY-SSW-DQC028], Beijing Municipal Science and Technology Commission [grant number Z181100002918003], and Guizhou Province Science and Technology Fund (grant number [2020]1Z035). The authors would like to thank Sen Hu, Yan Yang and Yongjiang Xu for academic consultation, and Yanxue Wu, Yang Li, Rui Li, Bing Mo, and Hong Jin for technical support.

References

Aines, R.D., Rossman, G.R., 1985. The high temperature behavior of trace hydrous components in silicate minerals. Am. Mineral. 70, 1169–1179.

Bradley, J.P., Ishii, H.A., Gillis-Davis, J.J., Ciston, J., Nielsen, M.H., Bechtel, H.A., Martin, M.C., 2014. Detection of solar wind-produced water in irradiated rims on silicate minerals. Proc. Natl. Acad. Sci. USA 111, 1732. https://doi.org/10.1073/pnas.1320115111.

Brunetto, R., Strazzulla, G., 2005. Elastic collisions in ion irradiation experiments: a mechanism for space weathering of silicates. Icarus 179 (1), 265–273.

Burke, D.J., Dukes, C.A., Kim, J.-H., Shi, J., Fama, M., Baragiola, R.A., 2011. Solar wind contribution to surficial lunar water: laboratory investigations. Icarus 211, 1082–1088. https://doi.org/10.1016/j.icarus.2010.11.007.

Cantando, E.D., Dukes, C.A., Loeffler, M., Baragiola, R.A., 2008. Aqueous depletion of Mg from olivine surfaces enhanced by ion irradiation. J. Geophys. Res. 113, E09011. https://doi.org/10.1029/2008JE003119.

Clark, R.N., 2009. Detection of adsorbed water and hydroxyl on the Moon. Science 326, 562–564. https://doi.org/10.1126/science.1178105.

Farrell, W.M., Hurley, D.M., Zimmerman, M.I., 2015. Corrigendum to solar wind implantation into lunar regolith: hydrogen retention in a surface with defects. Icarus 255, 116–126. https://doi.org/10.1016/j.icarus.2014.09.014.

Freeman, J.J., Wang, A., Kuebler, K.E., Jolliff, B.L., Haskin, L.A., 2008. Characterization of natural feldspars by Raman spectroscopy for future planetary exploration. Can. Mineral. 46, 1477–1500. https://doi.org/10.3749/canmin.46.6.1477.

Frogner, P., Broman, C., Lindblom, S., 1998. Weathering detected by Raman spectroscopy using Al-ordering in albite. Chem. Geol. 151, 161–168. https://doi.org/10.1016/s0009-2541(98)00077-1.

Greenwood, J.P., Itoh, S., Sakamoto, N., Vicenzi, E.P., Yurimoto, H., 2008. Hydrogen isotope evidence for loss of water from Mars through time. Geophys. Res. Lett. 35, 5. https://doi.org/10.1029/2007GL032721.

Greenwood, J.P., Itoh, S., Sakamoto, N., Warren, P., Taylor, L., Yurimoto, H., 2011. Hydrogen isotope ratios in lunar rocks indicate delivery of cometary water to the Moon. Nat. Geosci. 4, 79–82. https://doi.org/10.1038/ngeo1050.

Hendrix, A.R., Hurley, D.M., Farrell, W.M., Greenhagen, B.T., Hayne, P.O., Retherford, K.D., Vilas, F., Cahill, J.T.S., Poston, M.J., Liu, Y., 2019. Diurnally migrating lunar water: evidence from ultraviolet data. Geophys. Res. Lett. 46, 2417–2424. https://doi.org/10.1029/2018gl081821.

Holmes, H.F., Agron, P.A., Eichler, E., Fuller Jr, E.L., O'Kelley, G.D., Gammage, R.B., 1975. Alteration of an annealed and irradiated lunar fines sample by adsorbed water. Earth Planet. Sci. Lett. 28, 33–36. https://doi.org/10.1016/0012-821x(75)90070-9.

Hu, S., Lin, Y., Zhang, J., Hao, J., Feng, L., Xu, L., Yang, W., Yang, J., 2014. NanoSIMS analyses of apatite and melt inclusions in the GRV 020090 Martian meteorite: hydrogen isotope evidence for recent past underground hydrothermal activity on Mars. Geochim. Cosmochim. Acta 140, 321–333. https://doi.org/10.1016/j.gca.2014.05.008.

Hu, S., Lin, Y.T., Zhang, J.C., Hao, J.L., Yang, W., Deng, L.W., 2015. Measurements of water content and D/H ratio in apatite and silicate glasses using a NanoSIMS 50L. J. Anal. At. Spectrom. 30, 967–978. https://doi.org/10.1039/c4ja00417e.

Hu, S., Lin, Y.T., Anand, M., Franchi, I.A., Zhao, X., Zhang, J., Hao, J., Zhang, T., Yang, W., Changela, H., 2020a. Deuterium and ^{37}chlorine rich fluids on the surface of Mars: evidence from the enriched basaltic shergottite Northwest Africa 8657.J. J. Geophys. Res., Planets 125, 9. https://doi.org/10.1029/2020JE006537.

Hu, S., Lin, Y.T., Zhang, J.C., Hao, J.L., Yamaguchi, A., Zhang, T., Yang, W., Changela, H., 2020b. Volatiles in the martian crust and mantle: clues from the NWA 6162 shergottite. Earth Planet. Sci. Lett. 530, 115902. https://doi.org/10.1016/j.epsl.2019.115902.

Hurley, D.M., Sarantos, M., Grava, C., Williams, J.P., Retherford, K.D., Siegler, M., Greenhagen, B., Paige, D., 2015. An analytic function of lunar surface temperature for exospheric modeling. Icarus 255, 159–163. https://doi.org/10.1016/j.icarus.2014.08.043.

Ichimura, A.S., Zent, A.P., Quinn, R.C., Sanchez, M.R., Taylor, L.A., 2012. Hydroxyl (OH) production on airless planetary bodies: evidence from H^+/D^+ ion-beam experiments. Earth Planet. Sci. Lett. 345, 90–94. https://doi.org/10.1016/j.epsl.2012.06.027.

Johnson, E.A., Rossman, G.R., 2003. The concentration and speciation of hydrogen in feldspars using FTIR and ^{1}H MAS NMR spectroscopy. Am. Mineral. 88, 901–911. https://doi.org/10.2138/am-2003-5-620.

Johnson, E.A., Rossman, G.R., 2004. A survey of hydrous species and concentrations in igneous feldspars. Am. Mineral. 89, 586–600. https://doi.org/10.2138/am-2004-0413.

Jones, B.M., Aleksandrov, A., Hibbitts, K., Dyar, M.D., Orlando, T.M., 2018. Solar wind-induced water cycle on the Moon. Geophys. Res. Lett. 45, 10959–10967. https://doi.org/10.1029/2018gl080008.

Keller, L.P., McKay, D.S., 1997. The nature and origin of rims on lunar soil grains. Geochim. Cosmochim. Acta 61 (11), 2331–2341. https://doi.org/10.1016/S0016-7037(97)00085-9.

Kovács, I., Hermann, J., O'Neill, H.S.C., Fitz Gerald, J., Sambridge, M., Horvat, G., 2008. Quantitative absorbance spectroscopy with unpolarized light: Part II. Experimental evaluation and development of a protocol for quantitative analysis of mineral IR spectra. Am. Mineral. 93, 765–778. https://doi.org/10.2138/am.2008.2656.

Kronenberg, A.K., Yund, R.A., Rossman, G.R., 1996. Stationary and mobile hydrogen defects in potassium feldspar. Geochim. Cosmochim. Acta 62 (21), 4075–4094. https://doi.org/10.1016/S0016-7037(96)00249-9.

Li, S., Milliken, R.E., 2017. Water on the surface of the Moon as seen by the Moon Mineralogy Mapper: distribution, abundance, and origins. Sci. Adv. 3 (9), e1701471. https://doi.org/10.1126/sciadv.1701471.

Li, Y., Li, X., Wang, S., Li, S., Tang, H., Coulson, I.M., 2013. Crystal orientation results in different amorphization of olivine during solar wind implantation. J. Geophys. Res., Planets 118, 1974–1982. https://doi.org/10.1002/jgre.20151.

Liu, Y., Guan, Y., Zhang, Y., Rossman, G.R., Eiler, J.M., Taylor, L.A., 2012. Direct measurement of hydroxyl in the lunar regolith and the origin of lunar surface water. Nat. Geosci. 5, 779–782. https://doi.org/10.1038/ngeo1601.

Managadze, G.G., Cherepin, V.T., Shkuratov, Y.G., Kolesnik, V.N., Chumikov, A.E., 2011. Simulating OH/H_2O formation by solar wind at the lunar surface. Icarus 215, 499. https://doi.org/10.1016/j.icarus.2011.06.025.

McCord, T.B., Taylor, L.A., Combe, J.P., Kramer, G., Pieters, C.M., Sunshine, J.M., Clark, R.N., 2011. Sources and physical processes responsible for OH/H_2O in the lunar soil as revealed by the Moon Mineralogy Mapper (M3). J. Geophys. Res., Atmos. 116, E00G05. https://doi.org/10.1029/2010je003711.

Mosenfelder, J.L., Andrys, J.L., Handt, A.V.D., Kohlstedt, D.L., Hirschmann, M.M., 2020. Hydrogen incorporation in plagioclase. Geochim. Cosmochim. Acta 277, 87–110. https://doi.org/10.1016/j.gca.2020.03.013.

Nadeau, S.L., Epstein, S., Stolper, E., 1999. Hydrogen and carbon abundances and isotopic ratios in apatite from alkaline intrusive complexes, with a focus on carbonatites. Geochim. Cosmochim. Acta 63, 183–185. https://doi.org/10.1016/S0016-7037(99)00057-5.

Pieters, C.M., Goswami, J.N., Clark, R.N., Annadurai, M., Buratti, B., Combe, J.-P., Dyar, M.D., Green, R., Head, J.W., Hibbitts, C., Hicks, M., Isaacson, P., Kilma, R., Kramer, G., Kumar, S., Livo, E., Lundeen, S., Malaret, E., McCord, T., Mustard, J., Nettles, J., Petro, N., Runyon, C., Staid, M., Sunshine, J., Taylor, L.A., Tompkins, S., Varanasi, P., 2009. Character and spatial distribution of OH/H_2O on the surface of the moon seen by M^3 on Chandrayaan-1. Science 326, 568–572. https://doi.org/10.1126/science.1178658.

Poston, M.J., Grieves, G.A., Aleksandrov, A.B., Hibbitts, C.A., Dyar, M.D., Oralando, T.M., 2015. Temperature programmed desorption studies of water interactions with Apollo lunar samples 12001 and 72501. Icarus 255, 24–29. https://doi.org/10.1016/j.icarus.2014.09.049.

Schaible, M.J., Baragiola, R.A., 2015. Hydrogen implantation in silicates: the role of solar wind in Si-OH bond formation on the surfaces of airless bodies in space. J. Geophys. Res., Planets 119, 2017–2028. https://doi.org/10.1002/2014je004650.

Stephant, A., Robert, F., 2014. The negligible chondritic contribution in the lunar soils water. Proc. Natl. Acad. Sci. USA 111, 15007–15012. https://doi.org/10.1073/pnas.1408118111.

Sunshine, J.M., Farnham, T.L., Feaga, L.M., Groussin, O., Merlin, F., Milliken, R.E., Hearn, M.F., 2009. Temporal and spatial variability of lunar hydration as observed by the Deep Impact spacecraft. Science 326, 565–568. https://doi.org/10.1126/science.1179788.

Tartèse, R., Anand, M., Franchi, I.A., 2019. H and Cl isotope characteristics of indigenous and late hydrothermal fluids on the differentiated asteroidal parent body of Grave Nunataks 06128. Geochim. Cosmochim. Acta 266, 529–543. https://doi.org/10.1016/j.gca.2019.01.024.

Williams, J.P., Paige, D.A., Greenhagen, B.T., Sefton-Nash, E., 2016. The global surface temperatures of the moon as measured by the diviner lunar radiometer experiment. Icarus 283, 300–325. https://doi.org/10.1016/j.icarus.2016.08.012.

Wöhler, C., Grumpe, A., Berezhnoy, A.A., Shevchenko, V.V., 2017. Time-of-day–dependent global distribution of lunar surficial water/hydroxyl. Sci. Adv. 3, e1701286. https://doi.org/10.1126/sciadv.1701286.

Yan, B.K., Wang, R.S., Gan, F.P., Wang, Z.C., 2010. Minerals mapping of the lunar surface with Clementine UVVIS/NIR data based on spectra unmixing method and Hapke model. Icarus 208 (1), 11–19. https://doi.org/10.1016/j.icarus.2010.01.030.

Yang, Y., Liu, W.D., Qi, Z.M., Wang, Z.P., Smyth, J.R., Xia, Q.K., 2019. Re-configuration and interaction of hydrogen sites in olivine at high temperature and high pressure. Am. Mineral. 104 (6), 878–889. https://doi.org/10.2138/am-2019-6921.

Yoshida, T., Tanabe, T., Hirano, M., Muto, S., 2004. FT-IR study on the effect of OH content on the damage process in silica glasses irradiated by hydrogen. Nucl. Instrum. Methods Phys. Res., Sect. B 218, 202–208. https://doi.org/10.1016/j.nimb.2003.12.056.

Zeller, E.J., Ronca, J.B., Levy, P.W., 1966. Proton-induced hydroxyl formation on the lunar surface. J. Geophys. Res. 71, 4855–4860. https://doi.org/10.1029/jz071i020p04855.